

Effect of load-resisting force on photoisomerization mechanism of a single second generation light-driven molecular rotary motor

Cite as: J. Chem. Phys. 161, 164302 (2024); doi: 10.1063/5.0216074

Submitted: 27 April 2024 • Accepted: 30 September 2024 •

Published Online: 22 October 2024



View Online



Export Citation



CrossMark

Xiaojuan Pang,^{1,a)} Kaiyue Zhao,¹ Deping Hu,² Quanjie Zhong,¹ Ningbo Zhang,³ and Chenwei Jiang^{4,a)}

AFFILIATIONS

¹ School of Materials and Physics, China University of Mining and Technology, Xuzhou, Jiangsu 221116, People's Republic of China

² Center for Advanced Materials Research, Beijing Normal University, Zhuhai 519087, People's Republic of China

³ School of Mines, China University of Mining and Technology, Xuzhou, Jiangsu 221116, People's Republic of China

⁴ Ministry of Education Key Laboratory for Nonequilibrium Synthesis and Modulation of Condensed Matter, Shaanxi Province Key Laboratory of Quantum Information and Quantum Optoelectronic Devices, School of Physics, Xi'an Jiaotong University, Xi'an, Shaanxi 710049, People's Republic of China

Note: This paper is part of the JCP Special Topic on Molecular Dynamics, Methods and Applications 60 Years After Rahman.

^{a)} Authors to whom correspondence should be addressed: xiaojuan.pang@cumt.edu.cn and jiangcw@xjtu.edu.cn

ABSTRACT

A pivotal aspect of molecular motors is their capability to generate load capacity from a single entity. However, few studies have directly characterized the load-resisting force of a single light-driven molecular motor. This research provides a simulation analysis of the load-resisting force for a highly efficient, second-generation molecular motor developed by Feringa *et al.* We investigate the M-to-P photoinduced nonadiabatic molecular dynamics of 9-(2,3-dihydro-2-methyl-1H-benz[e]inden-1-ylidene)-9H-fluorene utilizing Tully's surface hopping method at the semi-empirical OM2/MRCI level under varying load-resisting forces. The findings indicate that the quantum yield remains relatively stable under forces up to 0.003 a.u., with the photoisomerization mechanism functioning typically. Beyond this threshold, the quantum yield declines, and an alternative photoisomerization mechanism emerges, characterized by an inversion of the central double bond's twisting direction. The photoisomerization process stalls when the force attains a critical value of 0.012 a.u. Moreover, the average lifetime of the excited state oscillates around that of the unperturbed system. The quantum yield and mean lifetime of the S₁ excited state in the absence of external force are recorded at 0.54 and 877.9 fs, respectively. In addition, we analyze a time-dependent fluorescence radiation spectrum, confirming the presence of a dark state and significant vibrations, as previously observed experimentally by Conyard *et al.*

Published under an exclusive license by AIP Publishing. <https://doi.org/10.1063/5.0216074>

I. INTRODUCTION

Molecules with photoisomerization capabilities upon radiation exposure hold potential for molecular switches and other devices.^{1–3} Such advancements contribute significantly to the field of quantum mechanochemistry.^{4,5} Quantum chemical methods allow microscopic observations of ultrafast processes, providing detailed insights into the isomerization mechanisms of molecular machines at a simulation level. Light-driven molecular motors convert light into mechanical energy through photoisomerization reactions and are viewed as potential power sources in artificial nanomechanical

systems. These motors, ranging from first^{6–8} to third generation and categorized by molecular configuration, engage in continuous unidirectional rotational motion. Feringa *et al.*^{9–13} have extensively reported on these configurations, which include the four-step, two-stroke,¹⁴ and three-stroke¹¹ motors incorporating photoisomerization and thermal isomerization processes or their combinations.^{15–18}

Recent advancements aim to enhance the quantum yield and rotational speed of these motors^{19,20} by strategies such as modifying the conical intersection^{21,22} through heterocyclic atom introduction or group substitution. These research works have led to the

discovery of novel phenomena, such as chiral pathways and periodic decay of molecular properties.²³ Studies by Olivucci *et al.* compared the quantum-classical dynamics of the natural visual pigment Rhodopsin and a synthetic biomimetic molecular rotor para-methoxy N-methyl indanylidene-pyrrolinium in methanol,²⁴ revealing that efficient light-energy conversion relies on the synchronization of rotary motion with auxiliary molecular vibrations at specific time points. Notably, ultrafast fluorescence upconversion spectroscopy by Conyard *et al.* revealed rapid fluorescence quenching and a fluorescence emission spectrum redshift during the M-to-P isomerization of the motor 9-(2-methyl-2,3-dihydro-1H-cyclopenta[a]naphthalen-1-ylidene)-9H-fluorene.^{25,26} A dark state emerged during this process, alongside a confirmed redshift through UV-pump/IR-probe spectroscopy. The redshift of the fluorescence emission spectrum has also been confirmed by the structure sensitivity and high time resolution of UV-pump/IR-probe spectroscopy in the experiment by Amirjalayer *et al.*,²⁶ and they suggest that the dark state may represent a new charge transfer excited state. However, theoretical calculations conducted by our group propose an alternative view, identifying the dark state generated during the P-to-M isomerization process as a region within the initial S₁ excited state with low oscillator strength rather than a distinct electronic state.^{27,28} Notably, the process we have focused on investigating is not the experimentally tested step but the half-cycle that has not been detected experimentally. In addition, another notable feature also observed by Conyard *et al.*²⁵ was the existence of strong oscillation in time-dependent integrated intensity and time-resolved mean frequency spectrum. However, to our knowledge, very few theoretical studies address the fluorescence quenching and oscillation phenomena associated with the M-to-P process of this molecular motor. Therefore, there is an urgent need to investigate the time-dependent fluorescence spectrum of the reverse photoisomerization process and explore its underlying mechanisms.

Furthermore, a significant obstacle in integrating molecular motors into molecular devices and utilizing them effectively lies in interfacing various functional nanometer-sized molecular devices and understanding their mechanisms and efficiency when incorporated into machinery. As these combined molecular devices are ultimately intended for application in the field of quantum mechanochemistry, it is imperative to investigate the ability to withstand external load-resisting forces and the impact of cargo weight on their mechanisms. While there have been numerous studies on the load-resisting capabilities of linear motors such as kinesin,^{29–37} research on the load capacity and response mechanisms of single-molecular motors under additional forces has received less attention. In experimental terms, several methods exist for effectively transferring forces from macroscopic systems to the molecular level. For instance, the atomic force microscopy (AFM) technique is used to tether macromolecules for conducting single molecule force spectroscopy (SMFS) experiments. Rief *et al.* have employed this technique to measure the mechanochemical properties of a critical part of muscle named titin,³⁸ indicating that the unfolding of titin can generate peak forces ranging from 150 to 300 pN. Wiita *et al.* investigated the reduction of sulfur–sulfur bonds by enzymes using an AFM setup,³⁹ demonstrating that mechanical force can induce the rupture of these covalent bonds in various instances.^{39–42} Over the past two decades, researchers have focused on the aspect of SMFS both experimentally^{43–45} and theoretically^{46,47} in

mechanobiology. Hugel *et al.*⁴⁸ designed a simple opto-mechanical device to investigate the influence molecule itself produced on the environment, with ~47 azobenzene serving as a key molecular actuator capable of exerting forces of ~200 pN on an AFM tip. Wang *et al.* explored the photomechanochemical and purely mechanical behaviors of azobenzene photoswitches under additional loads,³⁷ aiming to determine the threshold forces required to impede the photoisomerization of azobenzene molecules. Previous studies have primarily focused on identifying the critical external forces needed to prevent photoisomerization, with less emphasis placed on the effects of introducing load-resisting forces into the mechanism.

In this study, we investigated the complex photoisomerization mechanism of the light-driven molecular rotary motor, 9-(2,3-dihydro-2-methyl-1H-benz[e]inden-1-ylidene)-9H-fluorene, in the gas phase to determine the presence of fluorescent radiation during the dynamic M-to-P process. We employed the semi-empirical trajectory surface hopping method at the OM2/MRCI level. The relaxation of the M structure geometry from the Franck–Condon region on the S₁ excited state to the dark state occurs rapidly, followed by molecular evolution to the S₀ ground state through two distinct conical intersections after fluorescent radiation. Moreover, the effect of applied forces on photoisomerization dynamics was critically examined as it is essential for understanding the integration of light-driven rotary motors within molecular frameworks. Pioneering research by Valentini *et al.* demonstrated that applying tensile force on a simplified retinal chromophore model leads to a significant and counterintuitive increase in the trans-to-cis photoisomerization quantum yield.⁴⁹ This study also explores the influence of various load-resisting forces on the quantum yield, the average lifetime of the S₁ excited state, and the detailed mechanism of this molecular motor. A threshold value similar in magnitude to those reported in previous literature³⁷ was identified, impeding the isomerization process. This research conducted a preliminary investigation into the power stroke of a molecular motor under load-resistance conditions, laying a solid foundation for further examinations of the operational performance of various molecular motors.

The layout of this paper is as follows: Sec. II provides a brief overview of the semiclassical nonadiabatic molecular dynamics simulation method utilized. Detailed results and discussions of time-resolved fluorescence spectroscopy without load-resisting forces are presented in Sec. III. Research on the load-resisting capacity of molecular motors is presented in Sec. IV. Finally, summary and conclusions are provided at the end of this article.

II. METHODOLOGY

Nonadiabatic dynamics calculations and fluorescence radiation spectrum analyses were conducted using the development versions of the MNDO program⁵⁰ and the JADE package.⁵¹ The relevant energies, gradients, and nonadiabatic couplings were computed using the semi-empirical orthogonalization model 2 (OM2)^{52–54} at the multireference configuration interaction (MRCI)⁵⁴ level. This approach strikes a reasonable balance between computational expense and accuracy, having been validated in numerous photoinduced processes and compared against high-level calculations in previously published studies.^{53–61} Here, we also benchmark

the OM2/MRCI method with the high-level calculation method of CASPT2 (supplementary material, Fig. S4). The self-consistent field (SCF) calculations adhered to the Restricted Open-shell Hartree–Fock (ROHF) formalism, enhancing the accuracy of excited-state wave function descriptions when integrated with the MRCI method. The reference configurations for the MRCI expansion included the closed-shell ground state along with single and double excitations spanning from the highest occupied molecular orbital (HOMO) to the lowest unoccupied molecular orbital (LUMO). Both the minima energy geometries of the S_1 excited state and the S_0 ground state, as well as conical intersections (CIs), were optimized at the OM2/MRCI level using an active space of ten electrons across ten orbitals. In terms of the SCF configuration, it comprises the highest five occupied and lowest five unoccupied orbitals for the ground state, demonstrating effective energy convergence. The optimization processes for the S_0 ground state and S_1 excited state utilized the Newton–Raphson iteration scheme, while the CI-optimized structures were determined through analytically calculated gradients and nonadiabatic coupling vectors via the Lagrange–Newton method.⁶² Notably, the empirical decoherence correction proposed by Truhlar *et al.*⁶³ and Granucci *et al.*⁶⁴ to enhance the fewest switches scheme's internal consistency was not employed in this study.

The investigation into the M-to-P photoisomerization dynamics of the molecular motor was conducted using Tully's on-the-fly surface hopping method.⁶⁵ Samples with initial geometries and velocities were drawn from the Wigner distribution function based on the vibrational normal modes of the ground state M structure.^{62,66} Molecular dynamics simulations, starting from the Franck–Condon region on the S_1 excited state, were performed using the OM2/MRCI method with a time step of 0.1 fs for nuclear motion and a hundredfold smaller step for electronic propagation. The time-dependent fluorescence emission spectrum was compiled by aggregating the oscillator strengths from trajectories that remained on the S_1 excited state at the temporal time. The related energy, oscillator strengths, and current electronic state were all extracted from all of Tully's on-the-fly surface hopping results at each time. The detailed theory and arithmetic have been reported by the previously published work.⁶⁷

To explore the load-resistance capabilities of the molecular motor, a series of constant forces ranging from 0 to 0.012 atomic units (equivalent to 988.6 pN) were applied to atoms 10 and 26, simulating a “cargo” load. This range exceeds the force parameters of previous experiments, such as those by Hugel *et al.*,⁴⁸ where forces up to 500 pN did not inhibit the optical trans-*cis* isomerization reaction. Here, the range of forces that we applied to the current molecular motor (0.012 a.u. equal to 988.6 pN) is beyond the range of the existing experiments since the threshold value for the isomerization of the current molecular motor is tested to reach 0.012 a.u. A module within the JADE package facilitated the modification of applied forces during the simulations. This pair of opposite traction forces have always been applied constantly, regardless of the configuration changes of the molecular motor. The modified gradient force in every direction, such as x direction, can be simply expressed with: $F_{\text{new}}(x_i) = F_{\text{old}}(x_i) - f^*(x_j - x_i)/\sqrt{[(x_j - x_i)^2 + (y_j - y_i)^2 + (z_j - z_i)^2]}$. Here, i and j are the different atoms, f is the external force to be applied. This section analyzes the impact of external forces applied to specific atoms, namely, atoms 10 and 26,

on the molecular motor. Applying forces to these locations generates significant torques, potentially influencing the quantum yield and the photoisomerization mechanism. Such alterations could, in turn, affect the average rotational speed of the motor. The external forces are postulated to mimic the effects of “cargo,” where forces inducing a repulsive effect on isomerization can be generated through sonochemistry.^{49,68} The single molecular motor is covalently bonded to an AFM tip and a supporting glass slide to ensure robust attachment during these experiments.⁴⁸ This method of coupling and carrying “cargo” has been validated as an effective way to mimic the dragging forces and the isomerization process, as reported experimentally by Hugel *et al.*⁴⁸ and theoretically by Shao *et al.*⁶⁹

III. RESULTS AND DISCUSSION

The present study delves into the photoisomerization dynamics from M-to-P of the molecular compound 9-(2,3-dihydro-2-methyl-1H-benz[e]inden-1-ylidene)-9H-fluorene. The optimized molecular configurations and atom numbering are shown in Fig. 1. These geometries were optimized at the OM2/MRCI level. Optimization calculations were also performed using the GAUSSIAN 03 software package with a B3LYP/6-31G(d,p) basis set to confirm the reliability of the molecular motor geometries derived at this level.⁷⁰ Fundamental characteristic values, presented in Table 1 of our recent publication,²⁸ include the primary twisting angle of C8–C7–C18–C14, its adjacent dihedral angle, and bond lengths, which align well with the results from GAUSSIAN.

Notably, the pyramid dihedral angle C7–C4–C8–C18 for the S_0 ground state of the P structure is only -0.7° , indicating a planar configuration more so than the M structure (-1.6°), although both are below -2° . The method used to calculate the conical intersection structure involves tracking the minimum energy gradient, ensuring that the S_1 potential energy surface does not vary significantly along the path from P-to-M or M-to-P. The two optimized conical intersection structures align with the previously calculated results.²⁸ These structures feature distinct pyramid angles, with dihedral angles C7–C4–C8–C18 of -36.9° and 34.6° , respectively.

Although two conical intersections are identified from the P-to-M process study, only CI₁ primarily facilitates the nonadiabatic decay dynamics. The branch ratio of trajectories decaying to the ground state via the CI₁ channel accounts for 74.4%, significantly higher than the 25.6% via the CI₂ channel. Conversely, during the reverse P-to-M process, the branch ratios of trajectories hopping to the ground state through CI₁ and CI₂ are 92.8% and 1.50%, respectively. Notably, 48.5% of trajectories hop to the product P configuration via CI₁, while 82.6% decay to the P configuration through CI₂, even though the total number of trajectories involving CI₂ is less than CI₁.

To visualize these analytic hopping events, a schematic representation of the isomerization from M-to-P on the profiles of S_1 and S_0 potential energy surfaces is shown in Fig. 2(a). Initially at the optimized M(S_0) state, the population is vertically excited to the corresponding Franck–Condon region M(FC) on the S_1 excited state. The population then evolves along the potential energy surface²⁸ and decays to the optimized P(S_0) state through the conical intersection seam near the optimized CI₁ and CI₂ points. All significant points and indicated evolution paths are shown in

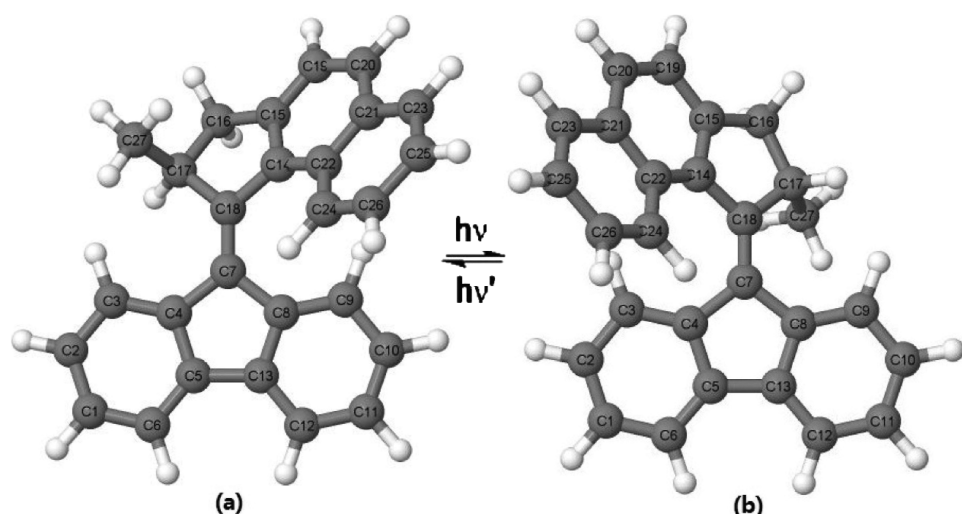


FIG. 1. Optimized geometries of (a) M and (b) P structures of molecular motor 1 calculated with the OM2/MRCI method. All the atoms are labeled.

Fig. 2(a). In addition, all critical hopping points are marked with red crosses on the two-dimensional contours of S_0 potential energy surfaces, calculated with the OM2/MRCI method as a function of two dihedral angles, C8–C7–C18–C18 and C7–C7–C8–C18,²⁸ as shown

in **Fig. 2(b)**. The hopping events are more accessible through the Cl_1 channel, consistent with our trajectory simulation results. Based on prior calculations, the total energy of Cl_2 is 6.99 kcal/mol higher than the corresponding Cl_1 structure, favoring evolution

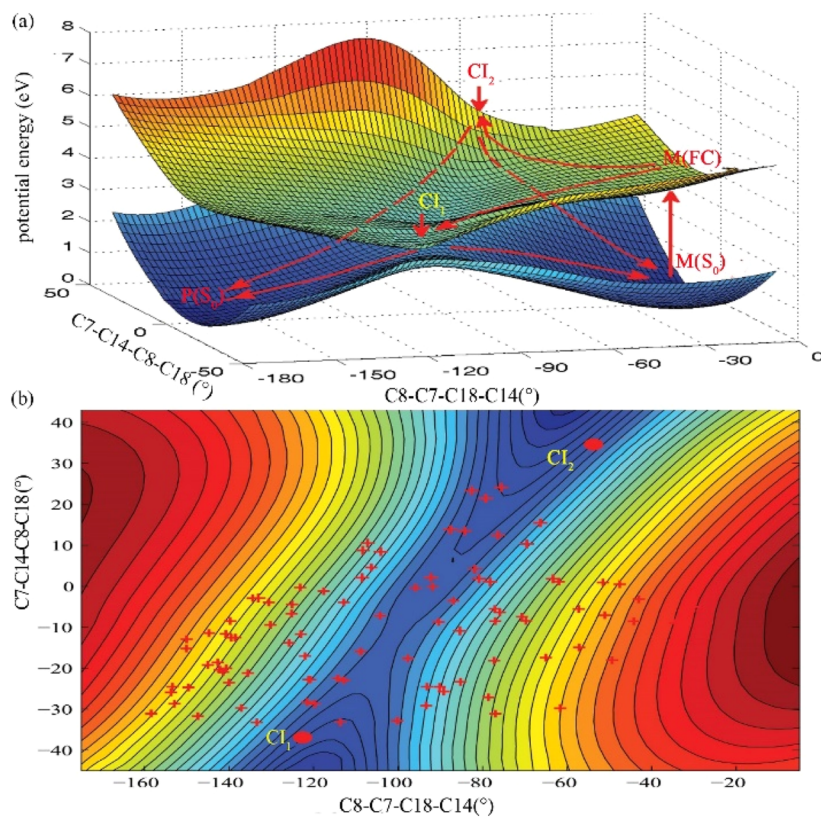


FIG. 2. (a) Schematic of isomerization from M-to-P on the profile of S_1 (upper) and S_0 (bottom) potential energy surface and (b) the hopping points on the two-dimensional contours of S_0 potential energy surfaces calculated with the OM2/MRCI method as a function of two dihedral angles of C8–C7–C18–C18 and C7–C7–C8–C18.²⁸

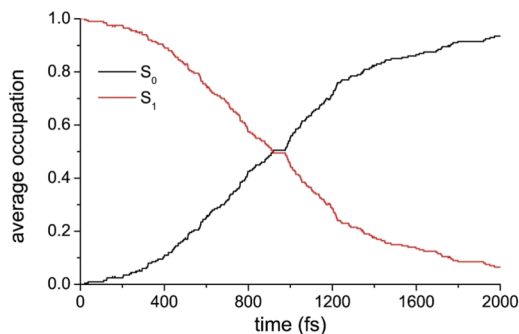


FIG. 3. Average occupation of the electronic states S_0 and S_1 as a function of simulation time during the M-to-P photoisomerization.

through the minimum energy path predominantly via the C_1 channel.

A. Pure M-to-P photoisomerization without load force

In this molecular dynamics simulation, 220 trajectories were derived from the Wigner distribution function, commencing at the Franck–Condon region of the S_1 state; the surface hopping dynamics of these trajectories were monitored over a 2000 fs duration. By the simulation's conclusion, 200 trajectories had decayed to the S_0 ground state, while the remaining 20 trajectories persisted in the S_1 state. Among the 200 trajectories that transitioned, 119 underwent M-to-P photoisomerization, yielding a quantum yield of 0.54 for

this process in the gas phase without any load force being applied. This quantum yield is notably higher than the experimentally detected result of 0.14, a disparity likely due to the simulations being conducted in a gas phase, while experimental observations were made in dichloromethane. Research by Filatov *et al.* corroborates that isomerization occurs faster and with greater quantum efficiency¹⁴ in a gas phase than in solution.

As shown in Fig. 3, the calculations indicate that the average S_1 lifetime for this process is ~ 877.9 fs, which is somewhat longer than the 710 fs observed for the reverse P-to-M process, as previously reported in our publications.²⁸ The de-excitation event initiates at 26.8 fs and continues until the simulation's end.

The emission of photons occurs when electrons transition from higher to lower energy levels, resulting in observable fluorescence, a phenomenon recently explored in experiments. Notably, the ultrafast time-resolved fluorescence caused by a substantial decrease in the oscillator strength in the excited state was observed.^{25,26} The process can be characterized by ultrafast fluorescence quenching, occurring within ~ 100 fs, and accompanied by strong oscillations.

To verify the existence of a dark state during the M-to-P isomerization process and its role in the mechanism, the emission spectrum of the molecule was generated by summing the vibrational strengths across the total population remaining on the S_1 potential energy surfaces at the corresponding times. The resultant spectrum, as shown in Fig. 4(a), shows a gradual decline in fluorescence over time with a quenching event at ~ 300 fs and notable oscillations during the process, highlighted in red at 25, 50, 75, and 125 fs. The peak fluorescence is $\sim 2.5 \times 10^4 \text{ cm}^{-1}$. Figure 4(b) shows a wavelength-resolved fluorescence emission spectrum from

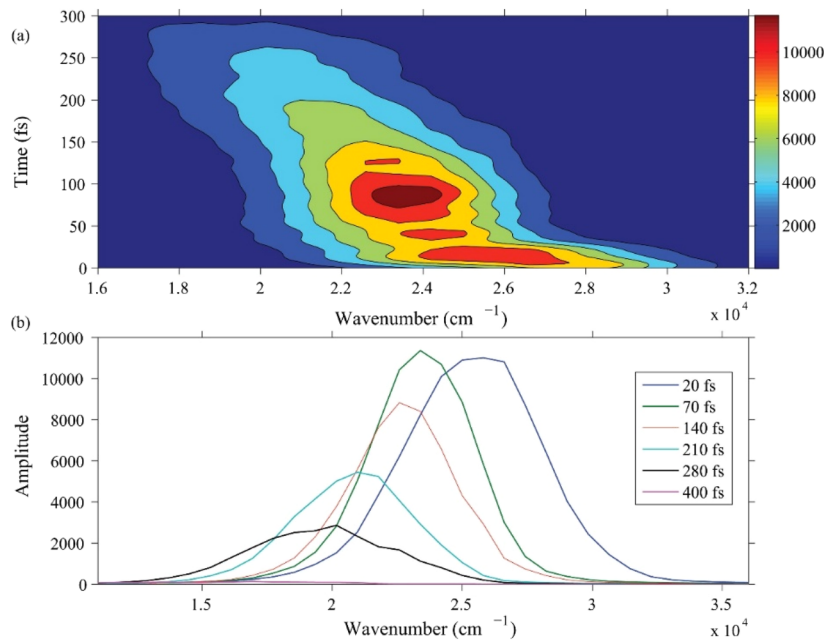


FIG. 4. Time-dependent fluorescence emission spectrum of the M-to-P photo-isomerization process of the molecular rotary motor. (a) Two-dimensional simulated contour of the emission intensity as a function of time and wavenumber. (b) Wavelength-resolved fluorescence emission spectrum calculated ranging from 20 to 400 fs over distinct intervals.

20 to 400 fs, displaying a redshift consistent with the declining oscillation intensity. Experimental observations indicate an ultrafast component within 100 fs and a temporal redshift in the emission spectra.²⁵ The strongest experimentally detected wavenumber is $\sim 2.0 \times 10^4 \text{ cm}^{-1}$, slightly lower than our theoretical results. Significant oscillations in the time-resolved emission were observed experimentally later (200, 400, 600, and 800 fs) compared to theoretical predictions. These discrepancies, such as the difference in ultrafast quenching time and peak wavenumber, may be attributable to the effects of the solvent, as theoretical calculations were conducted in the gas phase, while experimental observations used dichloromethane. The polar solvent's reorientation may stabilize the excited state, and its viscosity could influence the photochemical equilibrium of the molecular motor.⁷¹ In principle, the observed simulation results are in consistence with the results detected in the experiment.²⁵

With respect to the simulation time scale of 2 ps, the observed quenching time is considerably short and does not reach the average S_1 lifetime of 877.9 fs, suggesting that quenching occurs near the Franck–Condon section in the S_1 excited state. This implies that the isomerization mechanism involves the molecule entering a “dark state” and emitting photons from the Franck–Condon section in an ultrafast manner, followed by structural relaxation and evolution to the conical intersection before transitioning to the ground state, rather than undergoing a non-radiative process. It is important to note that the “dark state” referred to here does not signify a new electronic state but rather a region of the initial S_1 state with low oscillator strength.²⁸ The result agrees well with the previous conclusion that the strong oscillation phenomenon exists in this ultrafast fluorescence quenching process.²⁵

To further elucidate the relationship between molecular geometry and observed oscillator strength, time-dependent 3D trajectory

of a representative population during M-to-P photoisomerization were plotted as functions of the dihedral angles $C_8-C_7-C_{18}-C_{14}$ and $C_7-C_4-C_8-C_{18}$, with an inset graph showing the time-dependent $S_0 \rightarrow S_1$ oscillator strength. Before transitioning to the ground state, a reciprocating motion of population from the start point near the dark state is shown in Fig. 5. The hopping and start points are highlighted in the figure with a yellow block. The evolution process is accompanied by a large oscillation of the calculated oscillation strength, as shown in the inset illustration. A clear picture emerges that starting from the initial Franck–Condon region, a reciprocated motion of molecular around this section lasts about 700 fs, leading to the oscillation of the time-dependent $S_0 \rightarrow S_1$ oscillator strength during this time. For better understanding the reason of the decreased oscillator strength, the natural transition orbitals and geometries change at these different geometries, as well as the energy of higher S_2 state compared to that of S_1 state along the trajectory is calculated (supplementary material, Figs. S1–S3). The oscillations in fluorescence shown in Fig. 4 may thus reflect the corresponding vibrational motion of the molecular motor. Subsequently, ultrafast fluorescence quenching occurs, and the molecule evolves to the “dark state” until the hopping events emerge at 979.5 fs.

By comparing the results of two distinct isomerization processes in the gas phase for this specific molecular motor—namely, the P-to-M isomerization from previous studies and the reverse M-to-P isomerization from current work—we observed that ultrafast fluorescence quenching occurs in both scenarios. The quenching times for these processes are ~ 150 and 300 fs, respectively, which exceed the quenching time of 100 fs detected experimentally in dichloromethane. This variance suggests a solvent effect on the quenching dynamics.

The occurrence of a “dark state,” indicated by reduced oscillator strength between the S_1 and S_0 states, is further substantiated when compared to the average S_1 lifetimes of the two processes –710 fs for P-to-M and 877.9 fs for M-to-P. In addition, both processes exhibit a redshift in the emission photon's wavenumber, with the strongest central wavenumbers being quite close at 2.4×10^4 vs $2.5 \times 10^4 \text{ cm}^{-1}$, respectively.

A notable finding is that oscillations in fluorescence are observed only during the M-to-P isomerization process and not in the P-to-M process. This difference could be linked to the dynamics within the S_1 energy state. The slightly extended quenching time in the M-to-P process may provide additional opportunities for the molecule to enter a “bright state” during its population evolution on the S_1 energy surface before transitioning to the “dark state.” This behavior suggests a more dynamic interplay of electronic states during the M-to-P isomerization, possibly influenced by the specific pathway and molecular geometry involved in this direction of isomerization.

B. M-to-P photoisomerization under resisting force

To explore the power capability during the M-to-P isomerization process of the same molecular motor, a series of nonadiabatic dynamics simulations were conducted under varying external resisting loads. In particular, constant external load forces were applied to the rotor and stator portions of the molecular motor, specifically at atoms 26 and 10, as shown in Fig. 6. The selection of these

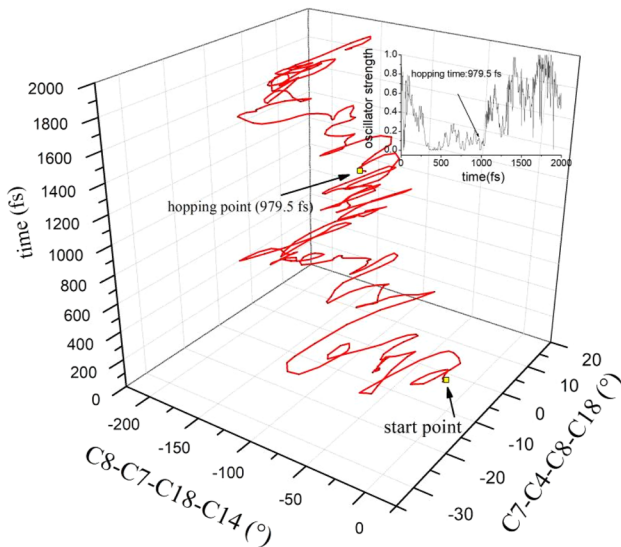


FIG. 5. Time-dependent 3D trajectory of a typical single representative population from M-to-P photo-isomerization as functions of $C_8-C_7-C_{18}-C_{14}$ and $C_7-C_4-C_8-C_{18}$, and the inset is the $S_0 \rightarrow S_1$ oscillator strength of the corresponding population.

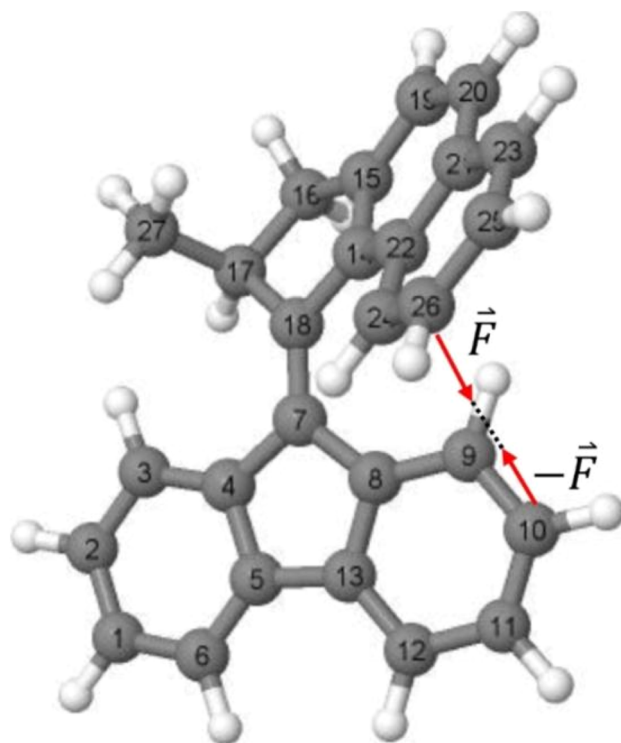


FIG. 6. Schematic illustration of the positions and orientation that the external forces added in the M structure of molecular motor in our extended simulation.

atom locations for applying load-resisting forces was based on previous theoretical⁶⁹ and experimental⁴⁸ studies that demonstrated their capability to generate substantial torque and effectively mimic the resistance forces that impede the rotational motion of an azobenzene motor.

Utilizing the same 220 samples initially extracted from the Wigner distribution function, pairs of opposite forces were artificially introduced to the molecule to study the effects of external forces. In prior experiments by Hugel *et al.*,⁴⁸ forces applied to individual polymers of an azobenzene switch ranged from 0 to 500 pN, with observations noting that optical trans-*cis* isomerization reactions ceased at forces exceeding 500 pN. However, in our simulations, the magnitude of the externally applied forces was set to range from 0 to 988.6 pN, increasing by increments of 82.4 pN (0.001 a.u.). Based on our simulation results, this adjustment identified 988.6 pN as the threshold force necessary to prevent photoisomerization events.

For each molecular dynamics simulation of the loaded motor under varying forces, the surface hopping dynamics were executed using the same 220 samples. The parameters used to investigate the detailed mechanism of photoisomerization were consistent with those described in the previous sections of this study. Intriguingly, the results indicated that external constraining forces significantly influenced the photoisomerization characteristics of the motor. Both the quantum yield and the isomerization mechanisms were notably affected, aligning with anticipated outcomes and corroborating initial reports by Valentini *et al.*⁴⁹

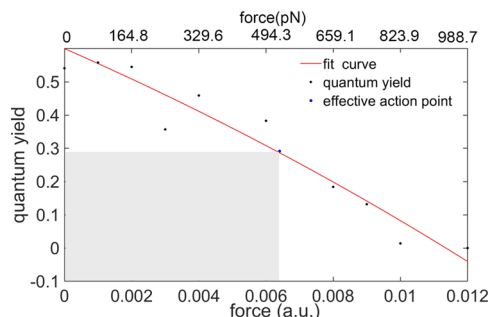


FIG. 7. Quantum yields scatter diagram and the fitting curve with the quadratic function of P structure molecular motor under different external forces ranging from 0 to 0.012 a.u. and the area calculated based on the most effective stress point shown in the blue star was 0.0064 a.u.

The relationship between various forces and their associated quantum yields is shown in Fig. 7, with values ranging from 0 to 0.012 a.u. As shown in Fig. 7, the black dots represent the quantum yields under different resisting forces, and the red solid line, which fits a quadratic trend function, accurately portrays the overall trend. The results demonstrate a decline in quantum yields as the magnitude of the load-resisting forces increases.

Notably, the observed decreasing trend in quantum yields is consistent across different fitting functions. In particular, the quantum yield remains relatively stable when the force magnitude is less than 0.003 a.u. Beyond this threshold, however, the quantum yield experiences a rapid quadratic decline as the external load-resisting forces increase. The relationship between the forces and the quantum yield can be described by a quadratic function $= -719.1x^2 - 43.8x + 0.5995$. Initially, a linear function was considered to model the impact of forces on quantum yield. However, the quadratic function yielded a residual norm value significantly lower than that of the linear model (0.006 019 vs 0.2693), suggesting a better fit with the quadratic function. As a result, the residual norm of the quadratic function is preferred for evaluating this relationship.

Based on these findings, a threshold value of 0.012 a.u. has been established to limit photoisomerization events. This indicates that the damping effect of the quantum yields follows a quadratic function as external forces increase. Moreover, the optimal constraining force, marked by a blue star on the red fitting line, is calculated to be 0.0064 a.u. At this point, within the gray rectangular region on the graph, there is maximum efficiency in restraining the molecular activity, as indicated by the largest area under the curve in Mathematica, highlighting the significant impact of this force on the molecular behavior.

We also examined the average lifetimes of the S_1 excited state under varying load-resisting forces, as shown by the black dots in Fig. 8. These data points, each representing one of 220 distinct samples subjected to forces ranging from 0 to 0.012 a.u., reveal that the average lifetime of the S_1 excited state generally fluctuates around 800 fs. Initially, the lifetime decreases with increasing forces up to 0.006 a.u. and then increases with further force application. The observed variability in the average lifetime of the S_1 state under

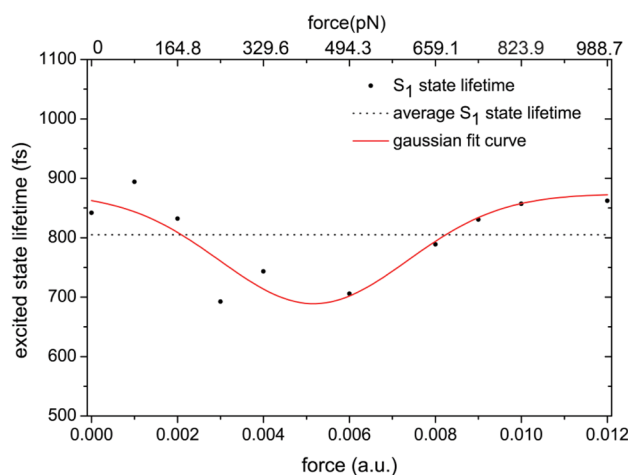


FIG. 8. Average S_1 excited state lifetime scatter diagram and their mean fitting line with the P structure molecular motor dragging under different external forces at disparate load-resisting forces.

different external forces clearly illustrates that these forces significantly affect the electron hopping time from the S_1 potential energy surface to the S_0 ground state, which could substantially influence the fluorescence spectrum.

The findings suggest that external forces below 0.006 a.u. may accelerate the isomerization process, potentially shortening the duration of the “dark state” in the molecular geometry on the S_1 potential energy surface. Conversely, when external forces exceed this threshold, the fluorescence is likely to gradually revert to its initial state.

To further understand the influence of external load-resisting forces on the photoisomerization mechanism of this molecular motor during the M-to-P process dynamics, we have analyzed two distinct mechanisms. Based on our statistical analysis, we selected two representative trajectories from the dynamics samples under external loading forces of 0.004 a.u. It is important to note that although a new type of photoisomerization mechanism was observed, these two mechanisms did not co-occur in the dynamic simulations.

When the load-resisting force is less than 0.003 a.u., the motor undergoes isomerization by twisting the pivotal C8–C7–C18–C14 dihedral angle in a clockwise direction to achieve the configuration of the product, as shown in Fig. 9(b). The pyramid dihedral angle C7–C4–C8–C18 also supports this isomerization process, as shown in Fig. 9(a). Observation of the spatial structure vibrations reveals that the pivotal C8–C7–C18–C14 dihedral angle successfully rotates to its ground state product configuration at 804.4 fs when the electron transitions from the excited to the ground state. As for bond-length vibrations, Fig. 10 shows that the central C7–C18 bond length is shortened during the hopping event, accompanied by an increase in the neighboring C7–C8 and C14–C18 bond lengths. The molecular geometry of the initial and product states is shown in inset of Fig. 9(b), with the direction of rotation marked by the red arrow. This electronic hopping to the ground state for isomerization aligns with our previous findings in the absence of a load-force. No

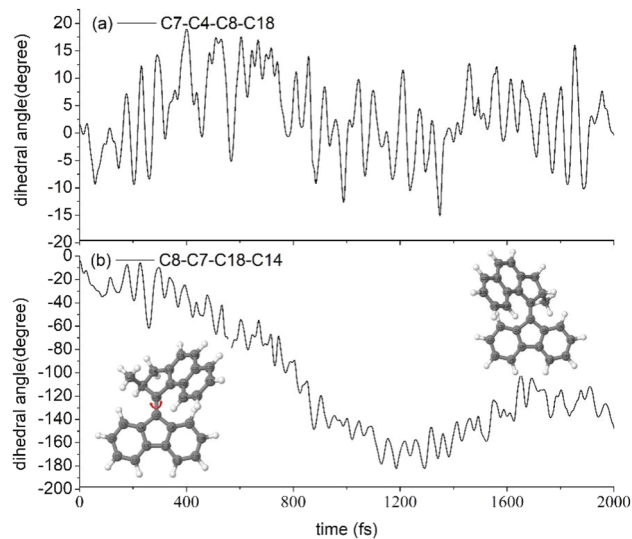


FIG. 9. Time dependence changes of (a) the central pyramid C7–C4–C8–C18 dihedral angle and (b) significate C8–C7–C18–C14 dihedral angle.

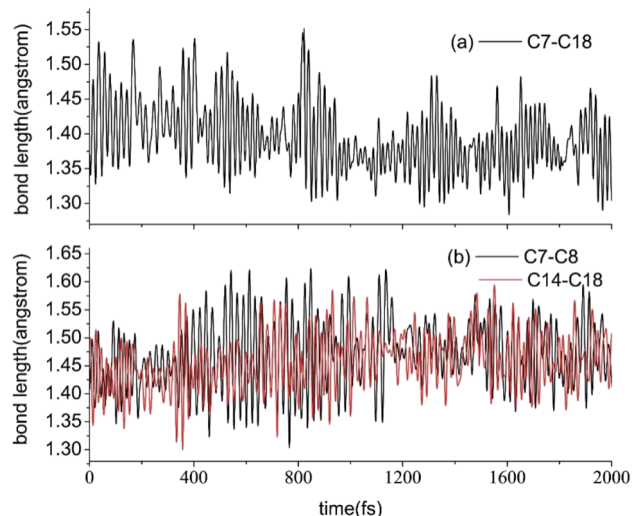


FIG. 10. Time dependence changes of its corresponding vibration motion of bond length (a) C7–C18 and (b) its adjacent bond lengths change of C7–C8 and C14–C18 in normal situations.

other novel mechanisms were observed until the load-resisting force surpassed 0.003 a.u.

However, when the magnitude of the forces is large enough to exceed this threshold (0.003 a.u.), a novel mechanism occurs. The direction of the large constraining external forces is opposite to that of photoisomerization, preventing the normal isomerization rotation and even reversibly pulling it back, thus providing kinetic energy for the motor to rotate in a counterclockwise direction. In addition, the sequential vibration of atoms reduces the spatial

repulsion between the stator and rotor at that moment, creating favorable conditions for the rotor to pass the stator. Notably, the stator portion of this molecular motor is characterized by spatial symmetry. Consequently, this new rotation method produces a final product with the same molecular conformation as traditional isomerization methods. In this sense, a new rotation mechanism was introduced under the load-resisting forces ranging from 0.003 to 0.010 a.u.

To comprehensively understand the newly observed photoisomerization mechanism, we show a single representative trajectory under external loading forces of 0.004 a.u. in Fig. 11. Figures 11(a) and 11(b) show that the main rotational movements involve the C8–C7–C18–C14 and the pyramid C7–C4–C8–C18 dihedral angles. Notably, the C8–C7–C18–C14 dihedral angle rotates in the opposite, counterclockwise direction and vibrates around this new value. However, it has not yet reached a stable equilibrium value at the time of the electron hopping event, indicating that the persistent counterclockwise rotation is indeed induced by the external forces applied. The molecular geometries of the initial and product points are shown in the inset of Fig. 11(b), with the rotation direction marked by the red arrow on the initial geometry.

Figure 12 shows the significant changes in bond lengths during the isomerization process. Similar to previous observations, the C7–C18 bond distance decreases while the C7–C8 and C14–C18 bond lengths increase. Over time, the central C7–C18 bond is compressed by the rotor and motor portions until it reaches a balanced value; when the electron transitions to the ground state, the molecule vibrates around this value. Conversely, the electron hopping weakens the bonding between adjacent atoms, increasing the C7–C8 and C14–C18 bond lengths.

As molecules evolve to a stable ground state, they vibrate around this new value. Notably, the isomerization process is halted when external forces are increased to 0.012 a.u., equivalent to

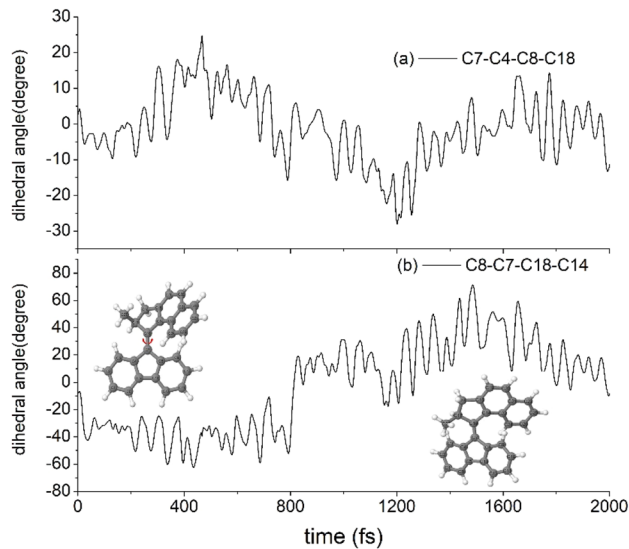


FIG. 11. Time dependence changes of (a) the central pyramid C7–C4–C8–C18 dihedral angle and (b) significant C8–C7–C18–C14 dihedral angle.

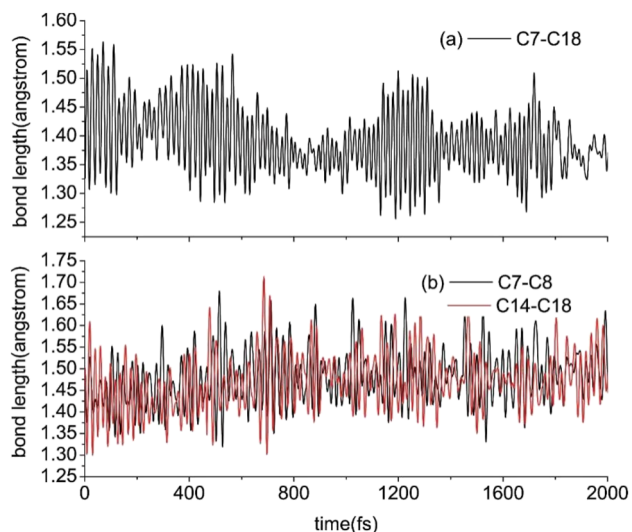


FIG. 12. Time dependence changes of its corresponding vibration motion of bond length (a) C7–C18 and (b) its adjacent bond lengths change of C7–C8 and C14–C18 in a novel situation.

988.6 pN. This threshold is consistent with the magnitude observed in previous studies by Hugel *et al.*⁴⁸ and Wang *et al.*⁶⁹ In the experiment by Hugel *et al.*, it was found that applying five additional pulses, exerting forces beyond 400 pN, did not result in a further shortening effect on the polymer to its *cis* state. They reported that the optical isomerization reaction of a single polyazoo peptide was absent at forces above 500 pN. Conversely, the simulations by Wang *et al.* indicated that photoisomerization could be inhibited by an external resisting force ranging from 90 to 200 pN (0.0011–0.0015 a.u.), while purely mechanical isomerization from the *cis* to trans-state could occur when the azobenzene molecule was subjected to a force of 1250–1650 pN (0.015–0.020 a.u.).⁶⁹

A vital feature of the new mechanism compared to traditional ones is the rotational orientation of the significant dihedral angle C8–C7–C18–C14. It is important to note that new rotational mechanism events occur if the external force applied exceeds 247.2 pN (0.003 a.u.). The simulation results showed that the molecular motor would overcome steric hindrances between the upper motor part and the bottom stator part, rotating directly in the opposite, counterclockwise direction under the influence of mechanical force. If the external forces exceed 988.7 pN, the isomerization process is interrupted. This observation predicts that similar isomerization mechanisms and associated ultrafast fluorescence quenching with a redshift could be observed in Hugel's experiments. Due to technical limitations in measuring the stopping force, their AFM experiments only detected the effects of external forces up to 400 pN, with a maximum pulling force limited to 1000 pN. Further technical advancements may enable exploration of the effects of repelling forces beyond 988.7 pN.

The symmetry of the stator portion and the reduction of spatial repulsion due to the load force facilitate this backward rotation, providing an efficient pathway for isomerization and direct access to the P spiral structure. Regarding the typical four-step molecular

motor designed by Feringa *et al.*, the motor can bypass the second step and jump directly from the first to the third step without undergoing the thermal reversal process, aided by the additional force applied at a specific location. This novel rotational phenomenon offers a way to adjust the rotational efficiency and quantum yield of light-driven molecular motors. The study of motor load carrying “cargo” holds promise, particularly if the impact of different forces applied at various positions can be further elucidated.

IV. CONCLUSIONS

In this study, we investigated the M-to-P photoisomerization dynamics and load-resisting capacity of 9-(2,3-dihydro-2-methyl-1H-benz[e]inden-1-ylidene)-9H-fluorene using on-the-fly surface-hopping dynamics at the semi-empirical OM2/MRCI level. The semiclassical simulation clearly shows that the photoisomerization reaction proceeds through twist in the central double bonds and along with the pyramid dihedral angle rotate. The simulation result of S₁ excited state lifetime was determined to be 877.9 fs, with two conical intersections identified as responsible for the isomerization.

An ultrafast quenching of the fluorescence spectrum was observed, calculated by summing the oscillator strengths across all trajectories remaining in the excited state. Time-dependent fluorescence spectroscopy revealed that the emission disappears at ~300 fs, characterized by strong oscillation and a redshift in the wavelength-resolved fluorescence emission spectrum. These observations suggest that the molecule transitions from the Franck–Condon region into a “dark state” immediately. This is followed by prolonged structural relaxation in the excited state and transitioning to the ground state via conical intersections. This indicates a rapid radiative process rather than non-radiative dynamics, providing substantial support for understanding the underlying mechanisms and aligning well with recent experimental results.

Furthermore, the load-resisting capacity of this molecular motor was explored, particularly in relation to its potential use in powering artificial nanomechanical applications. Simulations showed that photoisomerization of the motor is inhibited when external forces reach 0.012 a.u., and a new isomerization mechanism is triggered when the external resistance force reaches 0.003 a.u. The symmetrical nature of the stator causes the molecular motor to rotate in the opposite direction under these new conditions, reducing the product P configuration. The quantum yield of the M-to-P process exhibits a quadratic decline with increasing load-resistance forces, while the average lifetime of the S₁ excited state decreases initially up to 0.006 a.u. before increasing with further rises in the external force.

This research provides foundational support for investigating the ability of the molecule to function effectively in real hybrid systems and lays the groundwork for enhancing the performance of newly designed motor types.

SUPPLEMENTARY MATERIAL

The supplementary material contains the natural transition orbitals and geometries change at these different geometries, the energy of higher S₂ state compared to that of S₁ state along the trajectory, and benchmark calculation with OM2/MRCI against the CASPT2 method.

ACKNOWLEDGMENTS

This work was supported by the National Natural Science Foundation of China (Grant Nos. 12204532 and 52174137), the Natural Science Foundation of Jiangsu Province (Grant No. BK20200648), the Key Academic Project of China University of Mining and Technology (Grant No. 2022WLXK16), the Research Start-up Funding of China University of Mining and Technology (Grant No. 102519047), and the Graduate innovation project of China University of Mining and Technology (Grant No. 2024WLJCRCZL284). We thank Professor Zhengang Lan for providing the copyright of MNDO99 and JADE code.

AUTHOR DECLARATIONS

Conflict of Interest

The authors have no conflicts to disclose.

Author Contributions

Xiaojuan Pang: Conceptualization (equal); Methodology (equal); Writing – review & editing (equal). **Kaiyue Zhao:** Writing – original draft (equal). **Deping Hu:** Data curation (equal). **Quanjie Zhong:** Visualization (equal). **Ningbo Zhang:** Project administration (equal). **Chenwei Jiang:** Supervision (equal).

DATA AVAILABILITY

The data that support the findings of this study are available from the corresponding authors upon reasonable request.

REFERENCES

- Rivado-Casas, D. Sampedro, P. J. Campos, S. Fusi, V. Zanirato, and M. Olivucci, “Fluorenlylidene-pyrrolidine biomimetic light-driven molecular switches,” *J. Org. Chem.* **74**, 4666–4674 (2009).
- B. L. Feringa, “In control of motion: From molecular switches to molecular motors,” *Acc. Chem. Res.* **34**, 504–513 (2001).
- A. Singhania, S. Kalita, P. Chettri, and S. Ghosh, “Accounts of applied molecular rotors and rotary motors: Recent advances,” *Nanoscale Adv.* **5**, 3177–3208 (2023).
- C. L. F. van Beek and B. Feringa, “Coupled rotary motion in molecular motors,” *J. Am. Chem. Soc.* **146**, 5634–5642 (2024).
- L. Pfeifer, C. N. Stindt, and B. Feringa, “Coupled rotary and oscillatory motion in a second-generation molecular motor Pd complex,” *J. Am. Chem. Soc.* **145**, 822–829 (2023).
- T. R. Kelly, R. A. Silva, H. De Silva, S. Jasmin, and Y. Zhao, “A rationally designed prototype of a molecular motor,” *J. Am. Chem. Soc.* **122**, 6935–6949 (2000).
- T. R. Kelly, H. De Silva, and R. A. Silva, “Unidirectional rotary motion in a molecular system,” *Nature* **401**, 150–152 (1999).
- T. M. Neubauer, T. van Leeuwen, D. Zhao, A. S. Lubbe, J. C. M. Kistemaker, and B. L. Feringa, “Asymmetric synthesis of first generation molecular motors,” *Org. Lett.* **16**, 4220–4223 (2014).
- J. Vicario, A. Meetsma, and B. L. Feringa, “Controlling the speed of rotation in molecular motors. Dramatic acceleration of the rotary motion by structural modification,” *Chem. Commun.* **47**, 5910–5912 (2005).
- N. Komura, E. M. Geertsema, M. B. van Gelder, A. Meetsma, and B. L. Feringa, “Second generation light-driven molecular motors. Unidirectional rotation controlled by a single stereogenic center with near-perfect photoequilibria and acceleration of the speed of rotation by structural modification,” *J. Am. Chem. Soc.* **124**, 5037–5051 (2002).

- ¹¹J. C. M. Kistemaker, P. Stacko, J. Visser, and B. L. Feringa, "Unidirectional rotary motion in achiral molecular motors," *Nat. Chem.* **7**, 890–896 (2015).
- ¹²G. Srivastava, P. Stacko, J. I. Mendieta-Moreno, S. Edalatmanesh, J. C. M. Kistemaker, G. H. Heideman, L. Zoppi, M. Parschau, B. Feringa, and K. H. Ernst, "Driving a third generation molecular motor with electrons across a surface," *ACS Nano* **17**, 3931–3938 (2023).
- ¹³P. Roy, W. R. Browne, B. L. Feringa, and S. R. Meech, "Ultrafast motion in a third generation photomolecular motor," *Nat. Commun.* **14**, 1253 (2023).
- ¹⁴M. Filatov, M. Paolino, R. Pierron, A. Cappelli, G. Giorgi, J. Léonard, M. Huix-Rotllant, N. Ferré, X. Yang, D. Kaliakin *et al.*, "Towards the engineering of a photon-only two-stroke rotary molecular motor," *Nat. Commun.* **13**, 6433 (2022).
- ¹⁵C. García-Iriepa, M. Marazzi, F. Zapata, A. Valentini, D. Sampedro, and L. M. Frutos, "Chiral hydrogen bond environment providing unidirectional rotation in photoactive molecular motors," *J. Phys. Chem. Lett.* **4**, 1389–1396 (2013).
- ¹⁶L. Greb and J. M. Lehn, "Light-driven molecular motors: Imines as four-step or two-step unidirectional rotors," *J. Am. Chem. Soc.* **136**, 13114–13117 (2014).
- ¹⁷J. Ma, D. Zhao, C. Jiang, Z. Lan, and F. Li, "Effect of temperature on photoisomerization dynamics of a newly designed two-stroke light-driven molecular rotary motor," *Int. J. Mol. Sci.* **23**, 9694 (2022).
- ¹⁸K. Kuntze, D. R. S. Pooler, M. Di Donato, M. F. Hilbers, P. van der Meulen, W. J. Buma, A. Priimagi, B. L. Feringa, and S. Crespi, "A visible-light-driven molecular motor based on barbituric acid," *Chem. Sci.* **14**, 8458–8465 (2023).
- ¹⁹P. Roy, A. S. Sardjan, W. Danowski, W. R. Browne, B. L. Feringa, and S. R. Meech, "Control of photoconversion yield in unidirectional photomolecular motors by push-pull substituents," *J. Am. Chem. Soc.* **145**, 19849–19855 (2023).
- ²⁰N. Guo, B. Wang, and F. Liu, "Theoretical design and mechanistic study on a light-driven molecular rotary motor with B=N axis," *Acta Chim. Sin.* **76**, 196–201 (2018).
- ²¹M. Filatov and M. Olivucci, "Designing conical intersections for light-driven single molecule rotary motors: From precessional to axial motion," *J. Org. Chem.* **79**, 3587–3600 (2014).
- ²²J. Conyard, A. Cnossen, W. R. Browne, B. L. Feringa, and S. R. Meech, "Chemically optimizing operational efficiency of molecular rotary motors," *J. Am. Chem. Soc.* **136**, 9692–9700 (2014).
- ²³U. Muller and G. Stock, "Surface-hopping modeling of photoinduced relaxation dynamics on coupled potential-energy surfaces," *J. Chem. Phys.* **107**, 6230–6245 (1997).
- ²⁴A. Blanco-Gonzalez, M. Manathunga, X. Yang, and M. Olivucci, "Comparative quantum-classical dynamics of natural and synthetic molecular rotors show how vibrational synchronization modulates the photoisomerization quantum efficiency," *Nat. Commun.* **15**, 3499 (2024).
- ²⁵J. Conyard, K. Addison, I. A. Heisler, A. Cnossen, W. R. Browne, B. L. Feringa, and S. R. Meech, "Ultrafast dynamics in the power stroke of a molecular rotary motor," *Nat. Chem.* **4**, 547–551 (2012).
- ²⁶S. Amirjalayer, A. Cnossen, W. R. Browne, B. L. Feringa, W. J. Buma, and S. Woutersen, "Direct observation of a dark state in the photocycle of a light-driven molecular motor," *J. Phys. Chem. A* **120**, 8606–8612 (2016).
- ²⁷X. Pang, H. He, K. Zhao, N. Zhang, and Q. Zhong, "Ultrafast nonadiabatic photoisomerization dynamics study of molecular motor based on the synthetic indanylidene-ppyrrolinium frameworks," *Chem. Phys. Lett.* **819**, 140439 (2023).
- ²⁸X. Pang, X. Cui, D. Hu, C. Jiang, D. Zhao *et al.*, "Watching the dark state in ultrafast nonadiabatic photoisomerization process of a light-driven molecular rotary motor," *J. Phys. Chem. A* **121**, 1240–1249 (2017).
- ²⁹K. Svoboda and S. M. Block, "Force and velocity measured for single kinesin molecules," *Cell* **77**, 773–784 (1994).
- ³⁰H. Meyhöfer, "The force generated by a single kinesin molecule against an elastic load," *Proc. Natl. Acad. Sci. U. S. A.* **92**, 574–578 (1995).
- ³¹C. M. Coplin, D. W. Pierce, L. Hsu, and R. D. Vale, "The load dependence of kinesin's mechanical cycle," *Proc. Natl. Acad. Sci. U. S. A.* **94**, 8539–8544 (1997).
- ³²H. Kojima, E. Muto, H. Higuchi, and T. Yanagida, "Mechanics of single kinesin molecules measured by optical trapping nanometry," *Biophys. J.* **73**, 2012–2022 (1997).
- ³³K. Visscher, M. J. Schnitzer, and S. M. Block, "Single kinesin molecules studied with a molecular force clamp," *Nature* **400**, 184–189 (1999).
- ³⁴N. J. Carter and R. Cross, "Mechanics of the kinesin step," *Nature* **435**, 308–312 (2005).
- ³⁵A. Yildiz, M. Tomishige, A. Gennerich, and R. D. Vale, "Intramolecular strain coordinates kinesin stepping behavior along microtubules," *Cell* **134**, 1030–1041 (2008).
- ³⁶X. P. Hu, X. D. Zhao, I. Y. Loh, J. Yan, and Z. S. Wang, "Single-molecule mechanical study of an autonomous artificial translational molecular motor beyond bridge-burning design," *Nanoscale* **13**, 13195–13207 (2021).
- ³⁷W. W. Zheng, D. G. Fan, M. Feng, and Z. S. Wang, "The intrinsic load-resisting capacity of kinesin," *Phys. Biol.* **6**, 036002 (2009).
- ³⁸M. Rief, M. Gautel, F. Oesterhelt, J. M. Fernandez, and H. E. Gaub, "Reversible unfolding of individual titin immunoglobulin domains by AFM," *Science* **276**, 1109–1112 (1997).
- ³⁹M. F. Iozzi, T. Helgaker, and E. Uggerud, "Influence of external force on properties and reactivity of disulfide bonds," *J. Phys. Chem. A* **115**, 2308–2315 (2011).
- ⁴⁰P. Dopieralski, J. Ribas-Arino, P. Anjukandi, M. Krupicka, and D. Marx, "Force-induced reversal of β -eliminations: Stressed disulfide bonds in alkaline solution," *Angew. Chem. Int. Ed.* **55**, 1304–1308 (2016).
- ⁴¹H. Pei, M. Li, P. Wang, X. Yao, Z. Wen, and Z. Yue, "The effect of tensile stress on oxidation behavior of nickel-base single crystal superalloy," *Corros. Sci.* **191**, 109737 (2021).
- ⁴²P. Anjukandi, P. Dopieralski, J. Ribas-Arino, and D. Marx, "The effect of tensile stress on the conformational free energy landscape of disulfide," *PLoS One* **9**, e108812 (2014).
- ⁴³M. Rief, M. Gautel, A. Schemmel, and H. E. Gaub, "The mechanical stability of immunoglobulin and fibronectin III domains in the muscle protein titin measured by atomic force microscopy," *Biophys. J.* **75**, 3008–3014 (1998).
- ⁴⁴M. Grandbois, M. Beyer, M. Rief, H. Clausen-Schaumann, and H. E. Gaub, "How strong is a covalent bond?," *Science* **283**, 1727–1730 (1999).
- ⁴⁵J. N. Brantley, C. B. Bailey, K. M. Wiggins, A. T. Keatinge-Clay, and C. W. Bielawski, "Mechanobiophysics: Harnessing biomacromolecules for force-responsive materials," *Polym. Chem.* **4**, 3916–3928 (2013).
- ⁴⁶E. Evans and K. Ritchie, "Dynamic strength of molecular adhesion bonds," *Biophys. J.* **72**, 1541–1555 (1997).
- ⁴⁷I. Franco, C. B. George, G. C. Solomon, G. C. Schatz, and M. A. Ratner, "Mechanically activated molecular switch through single-molecule pulling," *J. Am. Chem. Soc.* **133**, 2242–2249 (2011).
- ⁴⁸T. Hugel, N. B. Holland, A. Cattani, L. Moroder, M. Seitz, and H. E. Gaub, "Single-molecule optomechanical cycle," *Science* **296**, 1103–1106 (2002).
- ⁴⁹A. Valentini, D. Rivero, F. Zapata, C. García-Iriepa, M. Marazzi, R. Palmeiro, I. F. Galván, D. Sampedro, M. Olivucci, and L. M. Frutos, "Optomechanical control of quantum yield in *trans-cis* ultrafast photoisomerization of a retinal chromophore model," *Angew. Chem. Int. Ed.* **56**, 3842–3846 (2017).
- ⁵⁰W. Thiel, *MNDO program, version 6.1*, Max-Planck-Institut für Kohlenforschung, Mülheim an der Ruhr, Germany, 2007).
- ⁵¹L. Du and Z. Lan, "An on-the-fly surface-hopping program JADE for non-adiabatic molecular dynamics of polyatomic systems: Implementation and applications," *J. Chem. Theory Comput.* **11**, 1360–1374 (2015).
- ⁵²E. Fabiano, T. Keal, and W. Thiel, "Implementation of surface hopping molecular dynamics using semiempirical methods," *Chem. Phys.* **349**, 334–347 (2008).
- ⁵³W. Weber and W. Thiel, "Orthogonalization corrections for semiempirical methods," *Theor. Chem. Acc.* **103**, 495–506 (2000).
- ⁵⁴N. Otte, M. Scholten, and W. Thiel, "Looking at self-consistent-charge density functional tight binding from a semiempirical perspective," *J. Phys. Chem. A* **111**, 5751–5755 (2007).
- ⁵⁵X. Zhuang, J. Wang, and Z. Lan, "Photoinduced nonadiabatic decay and dissociation dynamics of dimethylnitramine," *J. Phys. Chem. A* **117**, 4785–4793 (2013).
- ⁵⁶A. Kazaryan, Z. Lan, L. V. Schafer, W. Thiel, and M. Filatov, "Surface hopping excited-state dynamics study of the photoisomerization of a light-driven fluorene molecular rotary motor," *J. Chem. Theory Comput.* **7**, 2189–2199 (2011).

- ⁵⁷A. Nikiforov, J. A. Gamez, W. Thiel, and M. Filatov, "Computational design of a family of light-driven rotary molecular motors with improved quantum efficiency," *J. Phys. Chem. Lett.* **7**, 105–110 (2016).
- ⁵⁸B. Heggen, Z. Lan, and W. Thiel, "Nonadiabatic decay dynamics of 9H-guanine in aqueous solution," *Phys. Chem. Chem. Phys.* **14**, 8137–8146 (2012).
- ⁵⁹O. Weingart, Z. Lan, A. Koslowski, and W. Thiel, "Chiral pathways and periodic decay in *cis*-azobenzene photodynamics," *J. Phys. Chem. Lett.* **2**, 1506–1509 (2011).
- ⁶⁰S.-H. Xia, B.-B. Xie, Q. Fang, G. Cui, and W. Thiel, "Excited-state intramolecular proton transfer to carbon atoms: Nonadiabatic surface-hopping dynamics simulations," *Phys. Chem. Chem. Phys.* **17**, 9687–9697 (2015).
- ⁶¹Y. T. Wang, X. Y. Liu, G. Cui, W. H. Fang, and W. Thiel, "Photoisomerization of arylazopyrazole photoswitches: Stereospecific excited-state relaxation," *Angew. Chem.* **128**, 14215–14219 (2016).
- ⁶²M. Barbatti, G. Granucci, M. Persico, M. Ruckenbauer, M. Vazdar, M. Eckert-Maksic, and H. Lischka, "The on-the-fly surface-hopping program system NEWTON-X: Application to ab initio simulation of the nonadiabatic photodynamics of benchmark systems," *J. Photochem. Photobiol., A* **190**, 228–240 (2007).
- ⁶³C. Zhu, A. W. Jasper, and D. G. Truhlar, "Non-Born-Oppenheimer Liouville-von Neumann dynamics. Evolution of a subsystem controlled by linear and population-driven decay of mixing with decoherent and coherent switching," *J. Chem. Theory Comput.* **1**, 527–540 (2005).
- ⁶⁴G. Granucci, M. Persico, and A. Zoccante, "Including quantum decoherence in surface hopping," *J. Chem. Phys.* **133**, 134111 (2010).
- ⁶⁵J. Peng, Y. Xie, D. Hu, L. Du, and Z. Lan, "Treatment of nonadiabatic dynamics by on-the-fly trajectory surface hopping dynamics," *Acta Phys. -Chim. Sin.* **35**, 28–48 (2019).
- ⁶⁶J. E. Mayer and W. Band, "On the quantum correction for thermodynamic equilibrium," *J. Chem. Phys.* **15**, 141–149 (1947).
- ⁶⁷Z. Lan, Y. Lu, O. Weingart, and W. Thiel, "Nonadiabatic decay dynamics of a benzylidene malononitrile," *J. Phys. Chem. A* **116**, 1510–1518 (2012), Molecules, spectroscopy, kinetics, environment, and general theory.
- ⁶⁸S. Ding, W. Wang, A. Germann, Y. Wei, T. Du, J. Meisner, R. Zhu, and Y. Liu, "Bicyclo[2.2.0]hexene: A multicyclic mechanophore with reactivity diversified by external forces," *J. Am. Chem. Soc.* **146**, 6104–6113 (2024).
- ⁶⁹J. Shao, Y. Lei, Z. Wen, Y. Dou, and Z. Wang, "Nonadiabatic simulation study of photoisomerization of azobenzene: Detailed mechanism and load-resisting capacity," *J. Chem. Phys.* **129**, 164111 (2008).
- ⁷⁰M. Frisch, G. Trucks, H. Schlegel, G. Scuseria, M. Robb, J. Cheeseman, J. Montgomery, Jr., T. Vreven, K. Kudin, and J. Burant, *Gaussian 03, revision c. 02 2004*, Gaussian, Inc., Wallingford, CT, 2013.
- ⁷¹M. Klok, L. P. Janssen, W. R. Browne, and B. L. Feringa, "The influence of viscosity on the functioning of molecular motors," *Faraday Discuss.* **143**, 319–334 (2009).